3D MULTI-SLAB DIFFUSION-WEIGHTED READOUT-SEGMENTED ECHO-PLANAR IMAGING WITH REAL-TIME CARDIAC-REORDERED K-SPACE ACQUISITION

Robert Frost[1], Karla L. Miller[1], David A. Porter[2], Rob H. N. Tijssen[3], and Peter Jezzard[1]

[1]*FMRIB Centre, Nuffield Department of Clinical Neurosciences, University of Oxford, Oxford, United Kingdom,* [2]*Healthcare Sector, Siemens AG, Erlangen, Germany,* [3]*Department of Radiotherapy, UMC Utrecht, Utrecht, Netherlands*

Introduction Readout-segmented EPI (rs-EPI) improves diffusion-weighted (DW) image quality through multi-shot, navigated acquisition (1-4). A natural extension of this technique would be a 3D rs-EPI trajectory, enabling more efficient acquisition at SNR-optimal TRs (1-2s), acceleration along multiple dimensions and the acquisition of thin slices. However, the data acquisition and reconstruction must be designed to account for additional motion-induced phase gradients in the *z* direction. In addition, there are point-spread function (PSF) effects due to relaxation and the presence of any *k*-space discontinuities, which depend on the 3D readout trajectory. Recent work (5-8) has shown that motion artefacts can be controlled in multiple thin slab 3D acquisitions with single-shot readouts of single k_z partitions. We present a 3D, multi-slab version of rs-EPI in both simulation and experiment, and demonstrate reduced motion artefacts with real-time reordering of *k*-space to the cardiac cycle (2).

Theory *Acquisition schemes*: Figure 1a shows two possible *k*-space trajectories for the imaging and navigator data. The imaging trajectories cover 3D *k*-space over multiple TRs using either 2D or 3D segments (IM_{2D} and IM_{3D}), Similarly, either a 2D or a 3D navigator is acquired at the centre of 3D *k*-space for all shots (NAV_{2D} and NAV_{3D}). The simulated PSFs for IM_{2D} and IM_{3D} are shown in Fig. 1b and c, respectively. An IM_{3D}+NAV_{3D} scheme would allow 3D navigator phase correction; however, the PSF for the IM_{3D} trajectory (Fig. 1c) indicates aliasing and ghosting along *z*. The IM_{2D} PSF (Fig. 1b) indicates only minor blurring along *y*. Based on these simulations, we decided to pursue the IM_{2D} strategy. *Motion phase correction*: A computational model for brain motion during the cardiac cycle (5) was used to simulate motion-induced phase corruption of multi-shot DW rs-EPI. These simulations allowed evaluation of artefacts in IM_{2D} high-resolution imaging data in conjunction with NAV_{2D} and NAV_{3D} navigator trajectories. Synchronization of *k*-space acquisition with the cardiac cycle was also simulated, by preferentially choosing imaging segments closer to the centre of 3D *k*-space during diastole. In addition to placing the *k*-space centre during the cardiac "quiet phase", this ensures that motion corruption varies smoothly across *k*-space, minimizing discontinuities and periodicities. Motion artefacts were assessed by computing the voxel-wise temporal standard deviation (TSD) across 6 simulated repeats. Figure 2 demonstrates the 2D navigator correction with NAV_{2D} (similar NAV_{3D} results are not shown) and further artefact reduction with a cardiac-reordered *k*-space acquisition in a 2×2×2mm simulation with 8 k_z phase encodes.

Methods The IM_{2D}+NAV_{2D} acquisition approach was implemented experimentally by modifying a standard 2D rs-EPI sequence. Real-time *k*-space reordering was synchronized to the cardiac cycle using a pulse oximeter (2,10). To image efficiently at the SNR-optimal TR (1-2s), the acquisition uses multiple thin slabs with separate concatenations for odd and even slabs to reduce saturation effects at slab edges. Images were reconstructed using the following pipeline: phase correction, regridding, in-plane GRAPPA (11), navigator correction, segment concatenation, 3DFT and coil combination.

Experiments All scanning was conducted on a standard commercial 3T system. *Cardiac reordering validation*: 1.8×1.8×2mm data with b=1000s/mm^2 were acquired with 12 and 18 k_z phase-encodes using both sequential and cardiac-reordered *k*-space acquisitions. Other parameters were TR/TE=1000/87ms, α=68°, matrix=120×120, 5 readout segments, a single slab, 12-ch head coil. A b=0 volume and 6 DW volumes with diffusion encoding in the *z* direction (to give maximum motion sensitivity) were acquired. The voxel-wise coefficient of variation (CoV) was calculated across the 6 images to assess residual motion corruption. *Trace-weighted acquisition*: 1.5mm isotropic data with one b=0 volume and three b=1000s/mm^2 DW volumes with orthogonal encoding were acquired with 8 k_z phase encodes and cardiac-reordered *k*-space acquisition. Other parameters were TR/TE=1500/75ms, α=77°, matrix=144×144, 7 readout segments, R_{PE}=2 GRAPPA, 32-channel head coil, 10 slabs with 25% slab overlap and 10% k_z oversampling, scan time 11:30min. Trace-weighted images were calculated by taking the geometric mean of the DW images.

Results Figure 3 shows experimental results demonstrating the improvement with cardiac reordering in data with 18 k_z phase encodes (12 k_z data demonstrated even lower levels of artefact with cardiac reordering but the improvement in the 2D corrected DW images is clearer in the 18 k_z data). Similar to simulations (Fig. 2), the 2D-corrected DW images exhibit signal loss in central brain regions where there is most cardiac-related deformation. Using ROIs in the centre of images to calculate a mean TSD (simulation) or CoV (experiment), the cardiac reordering strategy demonstrates a reduction in motion phase artefacts by 40-50%. Multi-slab b=1000s/mm^2 trace-weighted data are shown in Fig. 4.

Discussion We have demonstrated the feasibility of a 3D multi-slab version of rs-EPI. Predictions in simulations were confirmed in experiment, namely successful 2D navigator correction and artefact reduction (40-50%) with a cardiac-reordered *k*-space acquisition. Simulations also indicated that reacquisition of the shots with the worst motion corruption would reduce motion artefacts further. GRAPPA undersampling of k_z phase-encodes is not possible due to the small *z* field of view of each slab; instead, a simultaneous multi-slab acceleration is presented elsewhere (12). Reacquisition and improved performance at slab interfaces will be the subject of further work.

Acknowledgements We are grateful for funding from the MRC. **References** (1) Robson MRM 1997. (2) Miller MRM 2003. (3) Nguyen ISMRM 1998. (4) Porter MRM 2009. (5) Frank NImg 2010. (6) Engström ISMRM 2010. (7) Van IEEE TMI 2011. (8) Engström ISMRM 2012. (9) Wirestam JMRI 1996. (10) Tijssen NImg 2011. (11) Griswold MRM 2002. (12) Frost submitted to ISMRM 2013.

Figure 1

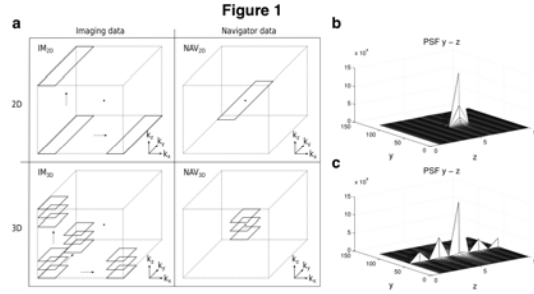

Figure 2

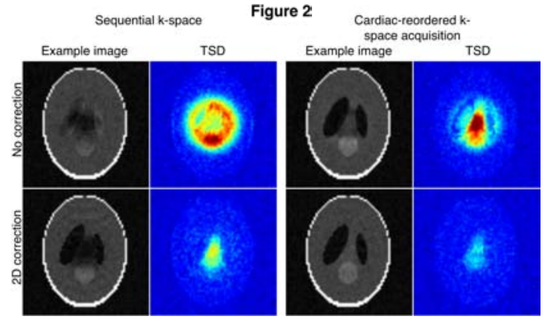

Figure 3

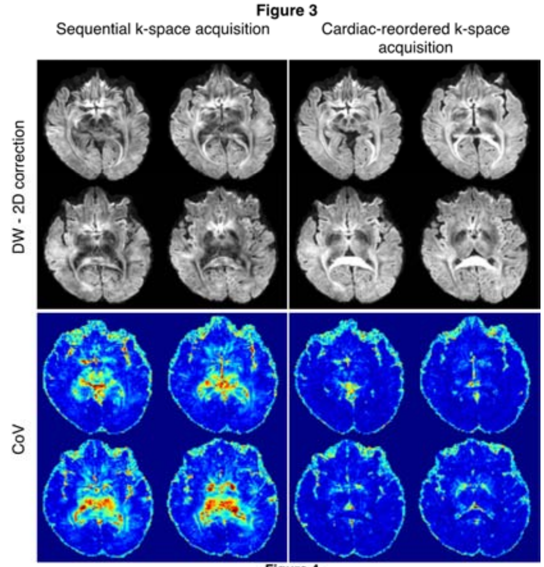

Figure 4